Dynamic pH Model for Autotrophic Growth of Microalgae in Photobioreactor: A Tool for Monitoring and Control Purposes

George A. Ifrim
LUNAM, Université de Nantes, ONIRIS, GEPEA, UMR-CNRS 6144, University Bd. CRTT-BP 406, 44600 Saint-Nazaire, Nantes, France

"Dunărea de Jos" University of Galaţi, Domnească Street, no. 47, 800008 Galaţi, Romania

Mariana Titica, Guillaume Cogne, Lionel Boillereaux, and Jack Legrand
LUNAM, Université de Nantes, ONIRIS, GEPEA, UMR-CNRS 6144, University Bd. CRTT-BP 406, 44600 Saint-Nazaire, Nantes, France

Sergiu Caraman
"Dunărea de Jos" University of Galaţi, Domnească Street, no. 47, 800008 Galaţi, Romania

DOI 10.1002/aic.14290
Published online November 29, 2013 in Wiley Online Library (wileyonlinelibrary.com)

A dynamic model for the photoautotrophic growth of microalgae in photobioreactor that describes the main variables of the system and allows the precise prediction of the pH in the culture was proposed and validated. The dynamic behavior of the biological system was expressed through a multistate model in continuous-time formulation, based on mass-balance equations and local photosynthetic responses of the anisotropic medium, further associated with a set of algebraic equations that describes the thermodynamic properties of the ammonia—carbon dioxide—water ternary solute system. The global photoautotrophic growth model was validated on experimental data acquired from a torus reactor inoculated with Chlamydomonas reinhardtii cells. The model response was studied in simulation for all identified input variables (dilution rate, incident light intensity, temperature, and flow rates of input gases). © 2013 American Institute of Chemical Engineers *AIChE J*, 60: 585–599, 2014

Keywords: pH modeling, photoautotrophic growth, carbon dioxide, ammonia, photobioreactor, total inorganic carbon

Introduction

Microalgae caught the attention of scientists and industrialists due to their simple growth requirements which make them potentially attractive for a wide range of applications. Species such as *Arthrospira* and *Chlorella* are already widely used in human and animal nutrition.[1] Microalgae can be metabolically redesigned as cell factories, thus proving useful in the biotechnological production of therapeutic and industrial metabolites such as long chain polyunsaturated fatty acids, pigments, polycarbohydrates, vitamins, and various biologically active compounds.[2,3] They can also be used in environmental applications such as greenhouse gas biomitigation, wastewater treatment processes, and biosorption of heavy metals.[4,5] The biomass resulted can be used in the production of biofuels (e.g., biodiesel, biohydrogen, bioethanol, and biogas),[6–9] an application that received increased attention for the past years.

Many of the algal groups are photoautotrophs, that is, they rely entirely on their photosynthetic apparatus to comply with their metabolic requirements. This type of organisms uses light, as source of energy, to convert CO_2 into organic substances. On the other hand, there is a large number of algal groups that contain photoheterotrophic species, able to acquire organic carbon from the external environment. However, only the photoautotrophs will be considered for modeling in this study, being of particular interest in the context in which the CO_2 production derived from human activities is increasing.

The sustainable development of pilot and industrial photobioreactors requires reliable monitoring and control tools to support the development of accurate operating protocols and achieve stable performance and process traceability. To this end, regarding the physicochemical and biological processes within the facility, quantifiable advanced knowledge is required.

The dynamic models which describe the behavior of microalgae cultures are usually a set of nonlinear differential equations mainly deduced from mass-balance considerations on both liquid and gaseous phases.

The light-driven processes of microalgae growth result in using a particular class of models yielding local photosynthetic responses by expressing the specific growth rate as a function of local irradiance for any depth of the culture. Thus, the radiative models, which express the light attenuation inside a culture of microalgae, are fundamental in

Correspondence concerning this article should be addressed to M. Titica at mariana.titica@univ-nantes.fr.

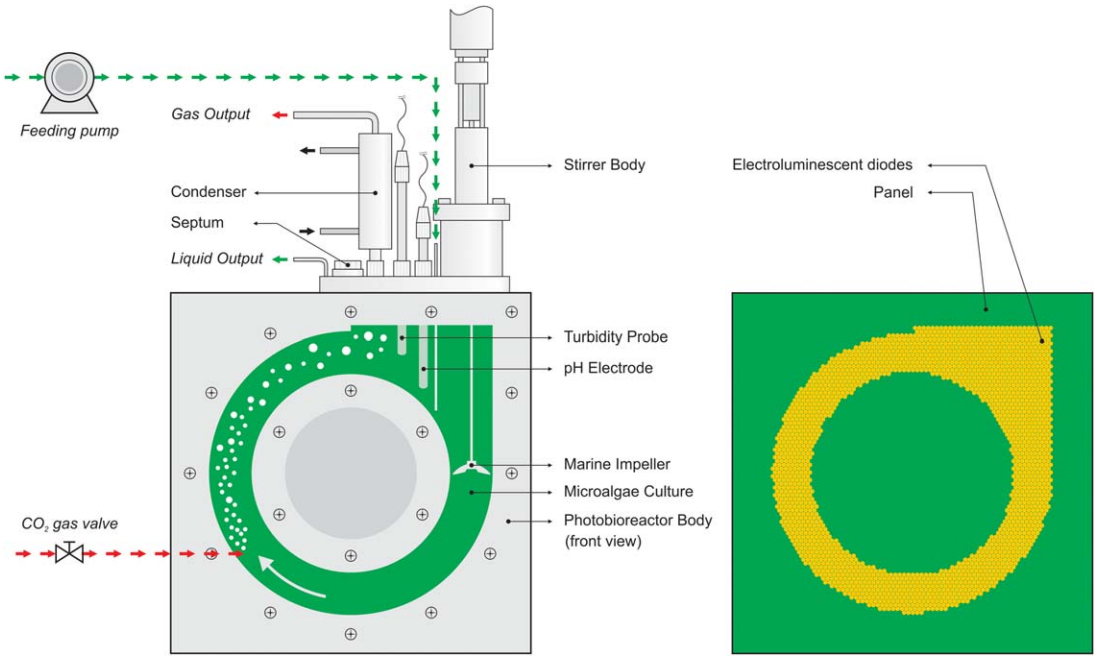

Figure 1. Torus photobioreactor.

The torus-shaped photobioreactor (left), developed by GEPEA Laboratory, was used in the experiments conducted for the validation of the global photoautotrophic growth model. The reactor, made of stainless steel, has a working volume of 1.47 L and a thickness of only 4 cm. It is lit on one side by means of an electroluminescent diode panel (right), whereas the back side is polished, giving a mirroring effect. The LED panel was conceived by attaching 750 white and 750 far-red diodes on a printed circuit. [Color figure can be viewed in the online issue, which is available at wileyonlinelibrary.com.]

photobioreactor studies. The coupling between radiative models and growth kinetics is an active research theme approached by various authors.[10–19]

The present research takes the mathematical modeling of the photoautotrophs' growth a step further by considering the chemical equilibria inside the culture broth, to allow an accurate prediction of pH under the influence of some of the most influential operating variables: CO_2 feeding, culture media feeding, culture media composition, incident light intensity, and temperature.

The photoautotrophic microorganisms are cultivated in aqueous solution in which the inorganic carbonaceous substrate is supplied through the dissolution of CO_2 gas in water or through the speciation of carbonates from the culture media. The dissolved carbon dioxide reacts with the water, forming ionic species such as bicarbonate (HCO_3^-) and carbonate (CO_3^{2-}) among which dynamic equilibria are established. The dissolved ammonia (NH_3) from the culture media reacts in its turn with the HCO_3^- ions to form carbamate ions (NH_2COO^-), thus composing a $NH_3-CO_2-H_2O$ ternary solute system. Most of the studies documented in the field of microalgae cultivation consider only the CO_2-H_2O solute system, even though the thermodynamic properties of the $NH_3-CO_2-H_2O$ ternary solute system have been extensively studied during the last decades due to their potential use in industrial and environmental applications such as urea and melamine production or CO_2 removal from flue gas in postcombustion carbon capture processes.[20,21] The ternary solute system is also considered for the aquaculture recycling installations.[22]

The present study proposes a global photoautotrophic growth model in which a radiative-transfer model, a biological model and a thermodynamic model are coupled. To this end, the article describes in detail the global model followed by validation on experimental data. The discussion focuses on model behavior emphasizing its usefulness as a tool for the monitoring and control of photobioreactors.

Materials and Methods

Biological agent and culture medium

In the experiments conducted for model validation, a wild type of *Chlamydomonas reinhardtii* strain 137AH was used, from a culture collection of the French Atomic Energy Center (Cadarache, France). Precultures were obtained incubating microalgae cells in conical flasks at 25°C and 100 μmol m^{-2} s^{-1} in standard Tris-acetate-phosphate medium with constant stirring. The inoculum for each experiment was obtained through centrifugal separation (2000 rpm, 5 min at 25°C) of precultures, the cell mass being resuspended in fresh autotrophic medium. The culture medium used for the photosynthetic growth of green algae in photobioreactor was an autotrophic minimum growth medium consisting of: $NaHCO_3$ (1.68 g L^{-1}), NH_4Cl (1.45 g L^{-1}), $MgSO_4 \cdot 7H_2O$ (0.28 g L^{-1}), $CaCl_2 \cdot 2H_2O$ (0.05 g L^{-1}), KH_2PO_4 (0.61 g L^{-1}), and Hutner's trace elements (1 mL L^{-1}).

Photobioreactor

The photobioreactor used in experiments is a lab-scale torus-shaped reactor, developed by the GEPEA laboratory, with a working volume of 1.47 L and a thickness of 4 cm. It has been described in detail elsewhere,[8] with the mention that, for this study, the incident light flux was provided by an electroluminescent diode panel calibrated with a LI-COR® light meter LI-1400 (Figure 1).

The incident light flux falls perpendicularly on one side of the reactor. The other side is made of polished stainless steel giving a mirror effect. The torus geometry associated with a

marine impeller confers a three-dimensional (3-D) vortex flow, adequate for the access of algae to the available light, ensuring a thorough homogenization of the medium.[23] This geometry allows considering that light attenuation is 1-D, facilitating the modeling of the light transfer attenuation.[15] For the addition of gasses (CO_2, N_2, or air), the reactor is provided with a microinjection system on the bottom.

Online measurements

The pH was measured with a Mettler Toledo® Inpro 3253SG/120/Pt100 electrode connected to a Mettler Toledo® pH2050e transmitter which gives an analog signal of 4–20 mA. The pH electrode is of gel-electrolyte type with an integrated Pt100 temperature sensor for automatic compensation.

The flow rates of the input (CO_2 and N_2) and the output gases were measured with three Bronkhörst® HIGH TECH EL-FLOW mass flow meters working at a maximum pressure of 2 bars:

1. Input mass flow meter calibrated for N_2 with the measuring range 0–100 mL min^{-1},
2. Input mass flow meter calibrated for CO_2 with the measuring range 0–3 mL min^{-1},
3. Output flow meter calibrated for CO_2 with the measuring range 0–100 mL min^{-1}.

The input mass flow meters are equipped with proportional control valves whose apertures are linearly dependent on their measuring range.

The composition of the output mixture of gases was determined by means of a QMS 200 PFEIFFER VACUUM® mass spectrometer calibrated for N_2, CO_2, O_2, and H_2. The measurement frequency of the gas samples requires a volume of 3–4 mL_n min^{-1}, which can be achieved by adding a vector gas (N_2).

Offline measurements

The dry matter of the culture was measured once a day, filtering a known volume of sample and weighing it before and after 24-h drying, in an oven, at 110°C. The fresh culture medium did not contain suspended solids and, therefore, the dry matter was associated with the biomass concentration. The total inorganic carbon (TIC) was measured on the supernatant with a Shimadzu® TOC-5000A analyzer. The preparation of the samples involved a centrifugation at 5000 rpm for 5 min and filtering when necessary.

Experimental protocol

The experiments were carried out at two different constant incident light intensities (100 and 300 μmol m^{-2} s^{-1}, respectively) operating the photobioreactor in discontinuous mode (dilution rate, $D = 0$). The CO_2 gas was bubbled into the culture at 3-h intervals, in pulses modulated to maintain a pH below 7.5. The temperature was kept constant at 25°C by means of an on-off controller that actuated a fan installed at the rear of the reactor. The signals transmitted by the components of the experimental assembly were acquired on a process computer which hosts the piloting program developed in LabVIEW®. The experimental data thus acquired were superimposed on simulations of the global photoautotrophic growth model computed with Matlab®.

The model was integrated with the experimental values of the feeding gas, the composition of the feeding gas and the corresponding experimental time, as input variables. The results obtained are presented graphically.

Bioprocess Modeling

Biological processes

The photoautotrophic microalgae are able to absorb CO_2 as major carbonaceous substrate and to generate O_2 as residue in the water oxidation reaction induced by light as source of energy. This type of organisms is cultivated in aqueous solution in which case the inorganic carbonaceous substrate is provided exclusively through CO_2 gas injection into the reactor or through carbonates addition into the culture medium. In water, the CO_2 gas forms other species such as dissolved carbon dioxide ($CO_{2,aq}$), carbonic acid (H_2CO_3), bicarbonate (HCO_3^-), and carbonate (CO_3^{2-}), whose sum is termed TIC. The ionic species represent potential sources of $CO_{2,aq}$ for photosynthesis as a result of their interconversion through a series of reactions such as hydration, dehydration, and protonation. The carbonates, usually used in research studies (e.g., sodium hydrogen carbonate—$NaHCO_3$, used in this case), have a similar behavior with respect to dissolution, forming the same species. The phase equilibrium (Eq. 1) is governed by Henry's law and is determined by the molality of the molecular solute. The vapor-phase dissociation of $CO_{2,aq}$ is significant only at very high temperatures and, therefore, can be neglected (P and T stand for pressure and temperature, respectively).[24]

$$CO_{2,gas} \overset{f(P,T)}{\longleftrightarrow} CO_{2,aq} \tag{1}$$

The weak electrolyte $CO_{2,aq}$ reacts with water, establishing the following chemical equilibria

$$CO_{2,aq} + H_2O \leftrightarrow H_2CO_3 \leftrightarrow H^+ + HCO_3^- \leftrightarrow 2H^+ + CO_3^{2-} \tag{2}$$

As it is hard to distinguish between $CO_{2,aq}$ and H_2CO_3, the two species will be referred to as a single dissolved gas.[22] The ratio between $CO_{2,aq}$ and HCO_3^- closely depends on pH, bicarbonate being the dominant species in solutions with pH above 6.3. The conversion of HCO_3^- into $CO_{2,aq}$ is very slow, being rapidly outrun by the photosynthetic consumption of $CO_{2,aq}$. Thus, when $CO_{2,aq}$ is removed from the medium, the equilibrium (Eq. 2) will shift to the left and the pH will increase. Many species of microalgae developed mechanisms that enable both $CO_{2,aq}$ and HCO_3^- to support photosynthesis,[25] but they still require $CO_{2,aq}$ which is obtained splitting the bicarbonate inside the cell ($HCO_3^- \leftrightarrow CO_{2,aq} + OH^-$), a reaction that releases hydroxyl ions (OH^-) causing an increase in pH. The culturing techniques of microalgae imply the pH control by means of CO_2 gas bubbled into the reactor. This fresh supply of CO_2 will shift the equilibrium back to the right, lowering the pH.

Besides the bicarbonate buffer system, the pH is also influenced by the ammonium ions (NH_4^+) present in the culture medium, which are in dynamic equilibrium (Eq. 3) with molecular ammonia (NH_3). The ratio of NH_4^+ to NH_3 closely depends on pH, ammonia being dominant in solutions with pH above 9.3. The selfionization of water must also be considered here (Eq. 4).

$$NH_3 + H_2O \leftrightarrow NH_4^+ + OH^- \tag{3}$$

$$H_2O \leftrightarrow H^+ + OH^- \tag{4}$$

NH_3 interferes with the HCO_3^- ions in solution forming carbamate. Thus, an additional equilibrium equation must be considered

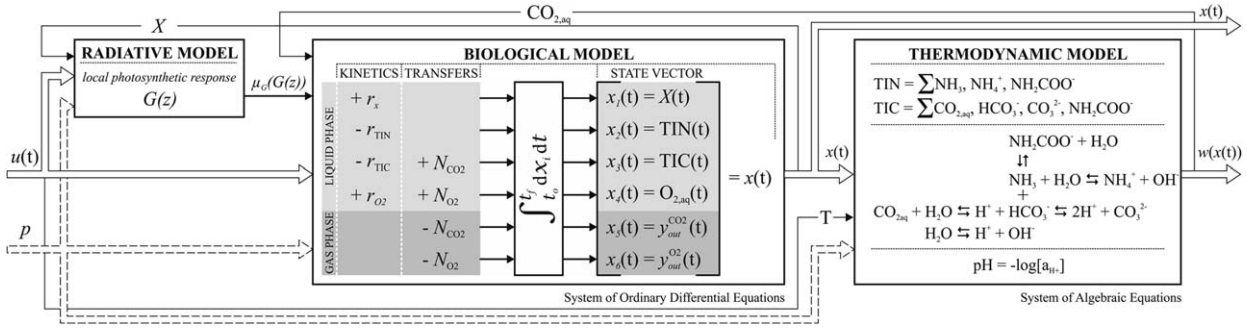

Figure 2. Structure of the global photoautotrophic growth model.

The global model that describes the photosynthetic growth of microalgae associates three models: a radiative model, a biological model, and a thermodynamic model. The radiative model describes the attenuation of light (G) along the culture depth (z) which, coupled with a kinetic expression, provides local photosynthetic responses, $\mu_G(G(z))$. The biological model balances kinetics of production (r_x and r_{O_2}) or consumption (r_{TIN} and r_{TIC}) and gas-liquid mass transfers (N_{O_2} and N_{CO_2}) to describe the six state variables of the system: biomass concentration, TIN concentration, TIC concentration, dissolved oxygen concentration, and CO_2 and O_2 molar fractions in the outlet gas. The thermodynamic model describes quantitatively the dissolved molecular and ionic species of the NH_3—CO_2—H_2O multisolute system and provides values of activity coefficients. $x^T = \left[X c_{TIN} c_{TIC} c_{O_2} y_{out}^{CO_2} y_{out}^{O_2}\right]$ is the state vector, $u^T = \left[q_0 D G_{in}^{CO_2} G_{in}^{O_2} G_{in}^{N_2} T\right]$ is the vector of inputs, $w^T = \left[c_{CO_2} c_{HCO_3^-} c_{CO_3^{2-}} c_{NH_3} c_{NH_4^+} c_{NH_2COO^-} c_{OH^-} c_{H^+} \mathrm{pH}\right]$ is the vector of internal variables and p is the set of model's parameters.

$$NH_3 + HCO_3^- \leftrightarrow NH_2COO^- + H_2O \quad (5)$$

The sum of NH_3, NH_4^+, and NH_2COO^- molar concentrations is termed total inorganic nitrogen (TIN).

Model structure and assumptions

The photosynthetic growth of microalgae under light-limiting conditions, along with the quantitative description of the chemical species described above, have been modeled associating three submodels briefly depicted in Figure 2, namely a radiative-transfer model, a biological model, and a thermodynamic model of the multicomponent system. The process being photoautotrophic, all biological phenomena described above are driven by the light available inside the culture (G) and, therefore, a radiative-transfer model is required to express its attenuation. As the culture is heterogeneous in terms of light availability, it is treated as a system with uniformly distributed parameters along its depth (z). The radiative-transfer model coupled with a kinetic law will provide local photosynthetic responses, $\mu_G(G(z))$, based on the input values of photon flux density, q_0, biomass concentration, X, and optical properties of the cultivated microorganism. However, the culture is considered well stirred and, therefore, homogeneous in terms of concentrations. As a result, the local photosynthetic responses are integrated to calculate the average photosynthetic response all over the volume of the reactor.

The biological model describes the time variation of main state variables of the system balancing kinetics of production or consumption and gas-liquid mass transfers. The state vector $x^T = \left[X\ c_{TIN}\ c_{TIC}\ c_{O_2}\ y_{out}^{CO_2}\ y_{out}^{O_2}\right]$ integrates six variables, namely biomass concentration, TIN concentration, TIC concentration, dissolved oxygen concentration, and CO_2 and O_2 molar fractions in the outlet gas; the first four are characteristic for the liquid phase, the last two being specific for the gaseous phase.

The thermodynamic model is a computational package that enables the quantitative description of dissolved molecular and ionic species of the $NH_3-CO_2-H_2O$ multisolute system and provides values of activity coefficients. The ternary solute system has been extensively studied over the last decades, the literature offering several models dedicated to the mathematical description of electrolyte solutions. A comparative study of thermodynamic electrolyte models was published by Jaworski et al.,[26] for the same system. Pitzer's ionic model,[27] which is a complex expansion of the excess Gibbs free energy that characterizes interactions among ions and solvent, was considered for this study. The thermodynamic model gives the vector of internal variables $w^T = \left[c_{CO_2} c_{HCO_3^-} c_{CO_3^{2-}} c_{NH_3}\ c_{NH_4^+}\ c_{NH_2COO^-}\ c_{OH^-}\ c_{H^+} \mathrm{pH}\right]$, variables which are functions of states (c is the concentration of chemical species i).

The vector of inputs $u^T = \left[q_0\ D\ G_{in}^{CO_2}\ G_{in}^{O_2}\ G_{in}^{N_2}\ T\right]$ includes some variables (i.e., q_0, D, and $G_{in}^{CO_2}$) with strong influence over the system that can be designated as control variables (with G_{in}^i being the input flow rate of gaseous component i—carbon dioxide, oxygen, and nitrogen).

p (as reported in Figure 2) is the set of model parameters which will be presented in the sections to follow.

Based on its geometry, it is safe to say that the reactor is perfectly stirred, and consequently the suspended algae can access the inorganic substrate and the dissolved gases equally to synthesize new cell mass. The nutrients (C, N, S, P sources) are considered to be in excess, but below inhibition levels, to express the specific growth rate as a function of light and not of chemical substrate, light being considered the limiting "substrate" that regulates the growth of photoautotrophs.

Radiative-transfer model

To determine the attenuation of light inside a photosynthetic culture, a radiative-transfer model (Eq. 6), designed for rectangular reactors lit on one side, was adopted. This model will determine the value of irradiance, G, for any depth, z, of the culture, through the following analytical solution

$$G(z) = 2q_0 \frac{(1+\alpha)e^{\delta(L-z)} - (1-\alpha)e^{-\delta(L-z)}}{(1+\alpha)^2 e^{\delta L} - (1-\alpha)^2 e^{-\delta L}} \quad (6)$$

with $\delta = X\sqrt{E_a(E_a+2bE_s)}$ the two-flux extinction coefficient and $\alpha = \sqrt{(E_a)/(E_a+2bE_s)}$ the linear scattering modulus. E_a

and E_s are the mass absorption and the mass scattering coefficients and b is the backward scattering fraction (dimensionless). q_0 represents the hemispherical incident light flux or photons flux density (PFD). X represents the biomass concentration inside the photobioreactor and L is the depth of the photobioreactor. The optical parameters can be determined spectrophotometrically for any given photosynthetic organism. This model is well documented, its parameters being identified for various microalgal species such as *Chlamydomonas reinhardtii*, *Spirulina platensis*, *Neochloris oleoabundans,* and so forth.[11,15–17,28]

Biological model

Photoautotrophic Growth Kinetics. The algal growth results from the difference between the anabolic and catabolic processes, in other words, the biomass increase through photosynthesis and the partial degradation through respiration. The global volumetric growth rate of photoautotrophs is expressed as follows

$$r_x = r_{x_p} - r_{x_s} = (\mu_G - \mu_s)X \tag{7}$$

with: r_{x_p}—the volumetric growth rate as a result of photosynthesis and r_{x_s}—the volumetric decline rate as a result of respiration. The specific growth rate related to photosynthesis, μ_G, is a function of the available light inside the culture and, therefore, a function of the local value of irradiance, $G(z)$. A Monod type model was used to represent the growth rate dependency on light

$$\mu_G = \mu_{\max}\frac{G}{K_I + G} \tag{8}$$

where K_I is the half-saturation constant and $\mu_{\max}$ is the maximum specific growth rate. The average photosynthetic response, $\langle \mu_G \rangle$, calculated for the entire volume of the reactor, is obtained by integrating the local photosynthetic responses along the culture depth, z

$$\langle \mu_G \rangle = \frac{1}{L}\int_0^L \mu_G(G(z))dz \tag{9}$$

where: $\langle\ \rangle$ denotes spatial averaging.

μ_s is a kinetic parameter related to the respiration process, described here as a constant maintenance term.

TIC Kinetics. The TIC consumption rate, $\langle r_{\mathrm{TIC}} \rangle$, is proportional to the global volumetric growth rate, $\langle r_x \rangle$. The biomass is synthesized exclusively from inorganic carbon (1 mol of CO_2 fixed leads to 1 C-mol biomass)

$$\langle r_{\mathrm{TIC}} \rangle = \frac{1}{M_x}\langle r_x \rangle = \frac{\langle \mu_G \rangle X - \mu_s X}{M_x} \tag{10}$$

where M_x is the C-mole mass.[29]

Stoichiometry of Photosynthetic Growth. The metabolism of photoautotrophic organisms is extremely complex and it is, therefore, difficult to derive kinetic equations for each substrate or product involved in the process. Whenever these components (e.g., nitrogen, phosphorus, oxygen, etc.) are neither limiting nor inhibiting the growth, the model can be reduced using a single stoichiometric equation and a single kinetic law that describes only the influence of light.

The overall stoichiometry of *Chlamydomonas reinhardtii* photosynthetic growth, which characterizes the yields of conversion of substrates into biomass and other products, based on the elemental conservation relationships (C, H, O, N, S, P), knowing that 1 mol CO_2 fixed leads to 1 C-mol biomass, is[30]

$$CO_2 + 0.576\ H_2O + 0.181\ NH_3 + 0.006\ H_2SO_4 + 0.021\ P_i \rightarrow CH_{1.771}O_{0.472}N_{0.181}S_{0.006}P_{0.021}(\mathrm{biomass}) + 1.107\ O_2 \tag{11}$$

After carbon, the TIN is considered to be the second main substrate that limits the photosynthetic growth of microalgae. Using an overall stoichiometric equation of the system, the TIN consumption rate $\langle r_{\mathrm{TIN}} \rangle$ can be computed as follows

$$\langle r_{\mathrm{TIN}} \rangle = \frac{Y_{N/X}}{M_x}\langle r_x \rangle \tag{12}$$

where $Y_{N/X}$ is the yield of TIN conversion which represents the rate of TIN uptake per unit of biomass produced.

The oxygen is produced through water photolysis and is partially consumed through respiration; its kinetic rate $\langle r_{O_2} \rangle$ is, therefore, proportional to the growth rate, as follows[30]

$$\langle r_{O_2} \rangle = \frac{Q_P}{M_x}\langle r_x \rangle \tag{13}$$

where Q_P is the photosynthetic quotient which represents the number of moles of O_2 produced divided by the number of moles of CO_2 (see Eq. 11).

Gas-liquid Mass Transfer. The gas-liquid mass transfer is modeled using the two-film theory, assuming that the gas phase is in plug flow and the liquid phase is well stirred. The volumetric mass-transfer rate for oxygen, N_{O_2}, can then be expressed as follows

$$N_{O_2} = (K_L a)_{O_2}\left(c^*_{O_2} - c_{O_2}\right) = (K_L a)_{O_2}\left(\frac{y^{lm}_{O_2} P}{H_{O_2}} - c_{O_2}\right) \tag{14}$$

where $c^*_{O_2}$ and c_{O_2} are the saturation and the actual concentrations of dissolved oxygen in the liquid phase. $(K_L a)_{O_2}$ is the overall volumetric mass-transfer coefficient for oxygen, $y^{lm}_{O_2}$ is the logarithmic mean (*lm*) between inlet and outlet oxygen molar fractions, and P is the total pressure in the gas phase. The Henry's constant, H_{O_2}, is estimated using the method given by Schumpe,[31] taking into account the decrease in solubility of gases determined by electrolytes in the culture medium.

In the same way, the volumetric mass-transfer rate for carbon dioxide N_{CO_2} is given by

$$N_{CO_2} = (K_L a)_{CO_2}\left(\frac{y^{lm}_{CO_2} P}{\gamma_{CO_2} H_{CO_2}} - c_{CO_2}\right) \tag{15}$$

where $(K_L a)_{CO_2}$, $y^{lm}_{CO_2}$, H_{CO_2}, and c_{CO_2} have the same meaning as above except that they are expressed for CO_2. $(K_L a)_{CO_2}$ is determined from the molecular diffusivities of carbon dioxide and oxygen (D_{CO_2} and D_{O_2}) by

$$(K_L a)_{CO_2} = (K_L a)_{O_2}\frac{D_{CO_2}}{D_{O_2}} \tag{16}$$

Thermodynamic Model—Multisolute System

In the $NH_3 - CO_2 - H_2O$ multisolute system, nine distinct species occur: NH_3 (molecular), NH_4^+, NH_2COO^-, CO_2 (molecular), HCO_3^-, CO_3^{2-}, H_2O (molecular), OH^- and H^+, resulting in 17 unknowns (c_i and γ_i for all species except water which is expressed in terms of activity, a_w). To solve these unknowns, 17 independent equations are needed:

1. Five chemical equilibria

$$K_1=\frac{a_{H^+}a_{HCO_3^-}}{a_{CO_2}a_w} \qquad K_2=\frac{a_{H^+}a_{CO_3^{2-}}}{a_{HCO_3^-}}$$

$$K_3=\frac{a_{NH_4^+}a_{OH^-}}{a_{NH_3}a_w} \quad K_4=\frac{a_{NH_3}a_{HCO_3^-}}{a_{NH_2COO^-}a_w} \tag{17}$$

$$K_w=\frac{a_{H^+}a_{OH^-}}{a_w}$$

where $a_i=\gamma_i\ c_i$ is the activity of component i, γ_i is the molal activity coefficient of component i, and c_i is the concentration of component i. The equilibrium constants K_1, K_2, K_3, K_4, and K_w in relation with temperature are available in literature.[24]

2. Two mass balances

$$c_{TIC}=c_{CO_2}+c_{HCO_3^-}+c_{CO_3^{2-}}+c_{NH_2COO^-} \tag{18}$$

$$c_{TIN}=c_{NH_3}+c_{NH_4^+}+c_{NH_2COO^-} \tag{19}$$

3. Electroneutrality relation:
The concentration of anions weighed by their charges must equal the concentration of cations weighed likewise.

$$c_{NH_4^+}+c_{H^+}+c_{Na^+}=c_{HCO_3^-}+2c_{CO_3^{2-}}+c_{NH_2COO^-}+c_{OH^-}+c_{Cl^-} \tag{20}$$

The electroneutrality is written for the main species present in the culture medium. The molar concentrations of the associated counterions Na^+ and Cl^- can be considered constant in the given experimental conditions.

4. In addition, Eq. 21 is used to calculate eight activity coefficients, one for each species except for water. Finally, Eq. 23 is used for the activity of water.

$$\begin{aligned}\ln\gamma_i=&-A_\phi z_i^2\left[\frac{\sqrt{I}}{1+1.2\sqrt{I}}+\frac{2}{1.2}ln\left(1+1.2\sqrt{I}\right)\right]\\&+2\sum_{j\neq w}m_j\left\{\beta_{ij}^0+\frac{\beta_{ij}^1}{2I}\left[1-\left(1+2\sqrt{I}\right)\exp\left(-2\sqrt{I}\right)\right]\right\}\\&-\frac{z_i^2}{4I^2}\sum_{j\neq w}\sum_{k\neq w}m_jm_k\beta_{jk}^1\end{aligned} \tag{21}$$

where $I=\frac{1}{2}\sum_j z_j^2m_j$, is the ionic strength of the solution. The parameters, β_{ij}^0 and β_{ij}^1, are molecule–molecule, molecule–ion, and ion–ion interaction parameters, given in Edwards et al.[24] A_ϕ (Debye–Hückel constant) can be expressed for temperatures ranging from 0 to 100°C with the following relation[32]

$$\begin{aligned}A_\phi=&-61.44534\ \exp\left(\frac{T-273.15}{273.15}\right)+2.864468\\&\left[\exp\left(\frac{T-273.15}{273.15}\right)\right]^2+183.5379\ ln\left(\frac{T}{273.15}\right)\\&-0.6820223(T-273.15)+0.0007875695\left(T^2-(273.15)^2\right)\\&+58.95788\left(\frac{273.15}{T}\right)\end{aligned} \tag{22}$$

The activity of water is determined from the Gibbs–Duhem equation

$$\begin{aligned}\ln a_w=M_w\Bigg\{&\frac{2A_\phi I^{\frac{3}{2}}}{1+1.2\sqrt{I}}-\sum_{i\neq w}\sum_{j\neq w}m_im_j\\&\left[\beta_{ij}^0+\beta_{ij}^1\exp\left(-2\sqrt{I}\right)\right]\Bigg\}-M_w\sum_{i\neq w}m_i\end{aligned} \tag{23}$$

Finally, the pH can be calculated with the following relation

$$pH=-\log\left(a_{H^+}\right) \tag{24}$$

Mass-Balance Model

The mass-balance model groups two types of components: conversion terms (which describe the kinetics of various biochemical reactions of the process and conversion yields of various substrates in terms of biomass and products) and terms for the dynamics of transport (which group transit of matter within the process in liquid or gaseous form, and transfer phenomena between phases).[33]

Liquid phase

The characteristic states for the liquid phase (X, c_{TIN}, c_{TIC}, and c_{O_2}), which describe the photoautotrophic growth process, are expressed in terms of mass-balance equations as follows

$$\frac{dX}{dt}=\langle r_X\rangle(t)-D(t)X(t) \tag{25}$$

$$\frac{dc_{TIN}}{dt}=-\langle r_{TIN}\rangle(t)+D(t)\left(c_{TIN,i}-c_{TIN}(t)\right) \tag{26}$$

$$\frac{dc_{TIC}}{dt}=-\langle r_{TIC}\rangle(t)+N_{CO_2}(t)+D(t)\left(c_{TIC,i}-c_{TIC}(t)\right) \tag{27}$$

$$\frac{dc_{O_2}}{dt}=\langle r_{O_2}\rangle(t)+N_{O_2}(t)-D(t)c_{O_2}(t) \tag{28}$$

where D represents the dilution, $c_{TIN,i}$ and $c_{TIC,i}$ represent the concentration of TIN and TIC, respectively, in the liquid feed. The rates $\langle r_X\rangle$, $\langle r_{TIC}\rangle$, $\langle r_{TIN}\rangle$, and $\langle r_{O_2}\rangle$ are given by Eqs. 7, 10, 12, and 13. The volumetric mass-transfer rates N_{O_2} and N_{CO_2} are given by Eqs. 14 and 15.

The biological model uses as input the dissolved carbon dioxide concentration—c_{CO_2} (required for the computation of N_{CO_2}) given by the thermodynamic model and determined through the mass balance Eq. 18. The concentration of ammonia, c_{NH_3}, is also determined using a mass balance Eq. 19. Water is expressed in terms of activity through Eq. 23. The concentrations of ionic species ($c_{HCO_3^-}$, $c_{CO_3^{2-}}$, $c_{NH_4^+}$, $c_{NH_2COO^-}$, and c_{OH^-}) present in the $NH_3-CO_2-H_2O$ ternary solute system can be computed from the chemical equilibria (17). The hydronium ions concentration, c_{H^+}, results from the electroneutrality Eq. 20 whose logarithm gives the pH (Eq. 24).

Gaseous phase

Based on the ideal gas law and gas balance equations, the molar fractions of the output gases can be computed, assuming that the flow and concentration of all inlet gases are known and measurable. Thus, the time variation of the specific states for the gas phase, $y_{out}^{CO_2}$ and $y_{out}^{O_2}$, is expressed by

$$\frac{dy_{out}^{CO_2}}{dt} = \frac{RT}{PV_g}\left(y_{in}^{CO_2}(t)G_{in}(t) - y_{out}^{CO_2}(t)G_{out}(t) - V_l N_{CO_2}(t)\right) \quad (29)$$

$$\frac{dy_{out}^{O_2}}{dt} = \frac{RT}{PV_g}\left(y_{in}^{O_2}(t)G_{in}(t) - y_{out}^{O_2}(t)G_{out}(t) - V_l N_{O_2}(t)\right) \quad (30)$$

where R is the universal gas constant, T is the temperature, and V_g and V_l are the gas and liquid volumes. G_{in} and G_{out} are the inlet and the outlet total flow rates.

A vector gas N_2 was present in the inlet gas and also in the outlet gas. N_2 gas has a lower solubility in water than CO_2 and O_2, and its volume is assumed to remain unchanged. It does not contribute to any consumption or production processes during the photoautotrophic growth. The N_2 molar fraction in the outlet gas, $y_{out}^{N_2}$, is given by

$$y_{out}^{N_2} = 1 - y_{out}^{CO_2} - y_{out}^{O_2} \quad (31)$$

All molar fractions in G_{in} are known

$$y_{in}^{CO_2} = \frac{G_{in}^{CO_2}}{G_{in}};\ y_{in}^{O_2} = \frac{G_{in}^{O_2}}{G_{in}};\ y_{in}^{N_2} = \frac{G_{in}^{N_2}}{G_{in}} \quad (32)$$

where $G_{in}^{CO_2}$, $G_{in}^{O_2}$, and $G_{in}^{N_2}$ are the feeding flow rates of CO_2, O_2, and N_2. G_{in} is the input gas flow rate and the sum of all input gases. The same relations can be written for the output gases; G_{out} can be calculated based on known input and output molar fractions of N_2

$$G_{out} = \frac{y_{in}^{N_2}}{y_{out}^{N_2}} G_{in} \quad (33)$$

Model Parameters

The parameters considered for the global photoautotrophic growth model presented above were already published in literature, most of them being identified on *Chlamydomonas reinhardtii* cultures. The model parameters can be divided into six groups:

1. Optical parameters (E_a, E_b, and b) used in the radiative model, measured in a previous study[15,17];
2. Kinetic parameters (μ_{max}, K_I, and μ_s), identified through multiparameter regression on experimental data in Fouchard et al.[17];
3. Yield conversion coefficients ($Y_{N/X}$ and Q_P), resulting from the stoichiometry equation;
4. Mass-transfer and diffusion coefficients: ($(K_La)_{O_2}$, D_{CO_2}, D_{O_2})—the overall volumetric mass-transfer coefficient for oxygen $(K_La)_{O_2}$ was determined in a previous study by Fouchard et al.,[17] for the same type of reactor, and the diffusion coefficients can be found in Denny[34];
5. Parameters characterizing the reactor geometry (V_l, V_g, and L), which are measurable;
6. Phase and chemical equilibria parameters (H_{CO_2}, H_{O_2}, K_1, K_2, K_3, K_4, and K_w)—Henry's constants are estimated through the method of Schumpe,[31] and the equilibrium constants are found in Edwards et al.,[24] at 25°C.

The parameters' values used in the numerical simulations of the photoautotrophic growth model are summarized in Table 1.

The global photoautotrophic growth model is highly sensitive to three parameters: μ_{max}, V_g, and $(K_La)_{O_2}$. μ_{max} was confirmed on offline experimental values of biomass, X, and incident light flux, q_0, and V_g was estimated by measuring the empty volume on the head of the reactor and on the gas lines, leaving $(K_La)_{O_2}$ the single parameter used to fit the model with the available experimental data. It is known that $(K_La)_{O_2}$ depends on a series of parameters related to the liquid-phase properties, the reactor's geometry, and the operating conditions. As the hydrodynamic conditions, the feeding gas flow rate, and the culture medium are the same in all experiments conducted for the validation of the global photoautotrophic growth model, $(K_La)_{O_2}$ was considered constant throughout this study. In addition, the culture medium properties remain unchanged under photoautotrophic conditions because the biomass concentration, the main component that modifies throughout the batch, does not alter the viscosity of the liquid and, therefore, the $(K_La)_{O_2}$.

Table 1. Model Parameters

Group	Parameter	Value	Unit
Radiative model	E_a	172	$m^2 \cdot kg^{-1}$
	E_b	870	$m^2 \cdot kg^{-1}$
	b	0.0008	–
Kinetic model	μ_{max}	0.16	h^{-1}
	K_I	120	$\mu mol \cdot m^{-2} \cdot s^{-1}$
	μ_s	0.013	h^{-1}
Stoichiometric values	$Y_{N/X}$	0.181	–
	M_x	$27.8 \cdot 10^{-3}$	$kg \cdot C\text{-}mole^{-1}$
	Q_P	1.107	–
Mass transfer and diffusion coefficients	$(K_La)_{O_2}$	0.9	h^{-1}
	D_{CO_2}	$1.92 \cdot 10^{-9}$	$m^2 \cdot s^{-1}$
	D_{O_2}	$2.38 \cdot 10^{-9}$	$m^2 \cdot s^{-1}$
Photobioreactor geometry	V_l	$1.47 \cdot 10^{-3}$	m^3
	V_g	$0.12 \cdot V_l$	m^3
	L	0.04	m
Phase and chemical equilibria	H_{CO_2}	2903.8	$Pa \cdot m^3 \cdot mol^{-1}$
	H_{O_2}	$8.385 \cdot 10^4$	$Pa \cdot m^3 \cdot mol^{-1}$
	K_1	$4.38 \cdot 10^{-7}$	–
	K_2	$4.65 \cdot 10^{-11}$	–
	K_3	$1.76 \cdot 10^{-5}$	–
	K_4	3.09	–
	K_w	10^{-14}	–
Other parameters	P	$1.013 \cdot 10^5$	Pa
	T	298.15	K
	R	8.3145	$J \cdot mol^{-1} \cdot K^{-1}$
	ct	$7.3 \cdot 10^3$	$mol \cdot L^{-1}$

The model and the experimental values achieved the best fitting for $(K_La)_{O_2} = 0.9\ h^{-1}$, a value that is not far from the one measured by Fouchard et al.,[17] namely 0.46 h^{-1} (for an air flow of 10 $mL_n\ min^{-1}$), for the same type of reactor and culture medium.

Yet, an empirical correlation (Eq. 34) that relates $(K_La)_{O_2}$ to U_G (superficial gas velocity) can be used instead, to increase the model predictability for a wider range of gas flow rates

$$(K_La)_{O_2} = mU_G^n \quad (34)$$

where m is a constant strongly affected by the gas injection system and the liquid medium. The exponent n can take values between 0.78 and 0.82 as presented in Shah et al.[35]

Nevertheless, when transferring the global photoautotrophic growth model on other reactors with different geometries, especially when scaled-up, complex models are recommended rather than empirical correlations. The substantial knowledge

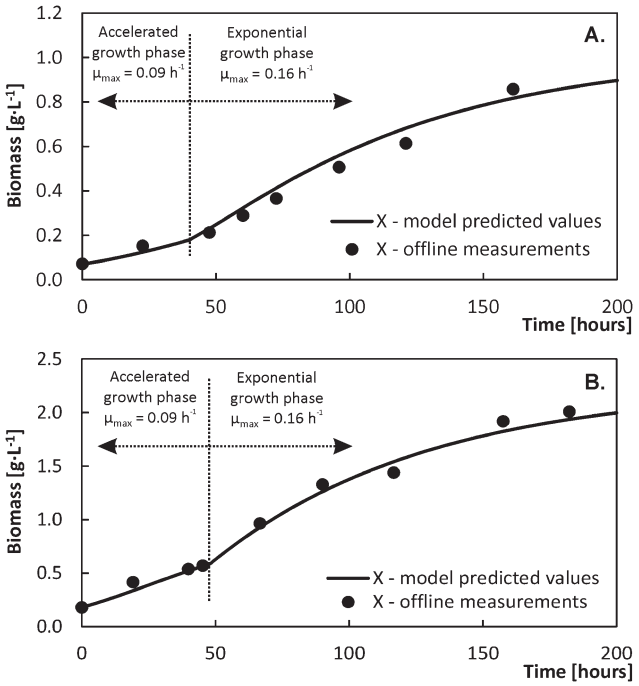

Figure 3. Biomass dynamics in photoautotrophic batch cultures.

The dynamics of the biomass concentration at (A) 100 μmol m^{-2} s^{-1} and (B) 300 μmol m^{-2} s^{-1} incident light intensity, measured offline (black dots), was compared with the response of the global photoautotrophic growth model (black line). Two growth phases with $\mu_{max}=0.09$ h^{-1} (during the first two days) and $\mu_{max}=0.16$ h^{-1} were identified. The model was initialized with the values presented in Table 2 and its parameters are rendered in Table 1.

regarding the gas-liquid mass transfer inside bioreactors can be easily adapted to photobioreactors. Mirón et al.,[36] for example, obtained good results on bubble column and airlift photobioreactors with an expression that relates $(K_La)_{O_2}$ to the superficial gas velocity, the overall gas holdup and the mean bubble diameter.

Results and Discussion

Model validation on Chlamydomonas reinhardtii photoautotrophic growth

Two experiments were conducted to validate the model described above, carried out at two different incident light intensities (110 and 300 μmol m^{-2} s^{-1}). The other culture conditions (e.g., substrate composition, temperature, stirring velocity, and feeding gas flow rate) were maintained identical in both experiments which ran for 200 h in discontinuous mode ($D=0$). It must be mentioned that the parameters that did have to be identified from the current experimental data were inferred from the data set acquired from the first experiment (Figures 3A, 4, and 5), whereas data set acquired from the second experiment (Figures 3B and 6) was used for model validation. As shown in Figures 3A and B, the microalgal culture presented a lag phase during the first 2 days. This behavior is also confirmed by the output O_2 gas dynamics, depicted in Figures 4C and 6C, respectively. To obtain a proper fitting of the global photoautotrophic growth model on experimental data, μ_{max} was considered equal to 0.09 h^{-1} during the first 40 h of cultivation for the first experiment and 48 h for the second one. However, from a technological point of view, low concentrations of biomass are of no interest and the accommodation phase is frequently neglected on the evidence that it is a short transitory phase and, therefore, zonal modeling oriented on the exponential growth phase is usually aimed. Implementing this model on other types of reactors and other species of photosynthetic organisms requires the reidentification of the optical and kinetic parameters.

To evaluate the pH response and the gas dynamics, the CO_2 was bubbled into the reactor by means of a pulse width modulation controller to maintain pH around 7.5. The amplitude of each CO_2 pulse corresponded to 100% aperture of the CO_2 proportional valve.

The input CO_2 gas (Figures 4A and 6A) was used as input variable in the global photoautotrophic growth model along with its corresponding acquired experimental time. The CO_2 used for this purpose was found to be impure, 2.8% being identified as O_2, which was also used as input variable in the model.

The input N_2 gas was also measured, and known to be constant at 10 mL min^{-1}. The volumetric flow rate of the output mixture of gases, G_{out}, was continuously measured, and the molar fractions of each component were analyzed through mass spectrometry. Thus, the partial volumes of each gas (except for $G_{in}^{N_2}$ known to be constant) are available.

Figures 4B and 6B show that the values predicted by the global model for the output rate of CO_2 are in good agreement with the experimental values acquired online for both experiments.

The output rate of O_2 (Figures 4C and 6C) was satisfactorily predicted in both experiments. The high values of output O_2 gas observed at the beginning of both experiments correspond to the air in the head of the reactor, which requires a certain time for complete depletion.

To implement the gas balance model on other types of reactors, it is necessary to adapt the liquid volume V_l, the gas volume V_g, and the volumetric mass-transfer coefficient $(K_La)_{O_2}$ to the new technological conditions. The V_l/V_g ratio has a strong influence on the gaseous phase—output CO_2 and O_2 gas dynamics—and no influence on the liquid phase, as V_l is always constant (for both batch and continuous cultures). A higher ratio (thus, a higher V_g) tends to predict lower output gas values than those in practice. V_g was approximated to 12% of V_l counting the reactor head and the gas lines up to the measuring device. The volumetric mass-transfer coefficient $(K_La)_{O_2}$, on the other hand, influences the variables related to the liquid phase (TIC, $CO_{2,aq}$, $O_{2,aq}$, and implicitly the pH).

A set of offline measurements for TIC is available only for the experiment piloted at 110 μmol m^{-2} s^{-1} incident light intensity. Figure 5 shows a close agreement between the predicted and the experimental values, with an error of at most 10% (see error bars). The dominant species of TIC is the HCO_3^- which represents approximately 95% at a pH close to 7.5, thus making the $CO_{2,aq}$ contribution very low, which is why the TIC expression is insensitive to $(K_La)_{O_2}$ variations over a broad range. Conclusively, the lack of data for $CO_{2,aq}$ and $O_{2,aq}$ narrowed the reidentification of $(K_La)_{O_2}$ solely based on the pH dynamics (known to depend closely on $CO_{2,aq}$).

The model tends to predict higher values for the pH during the first hours of cultivation (Figures 4D and 6D,

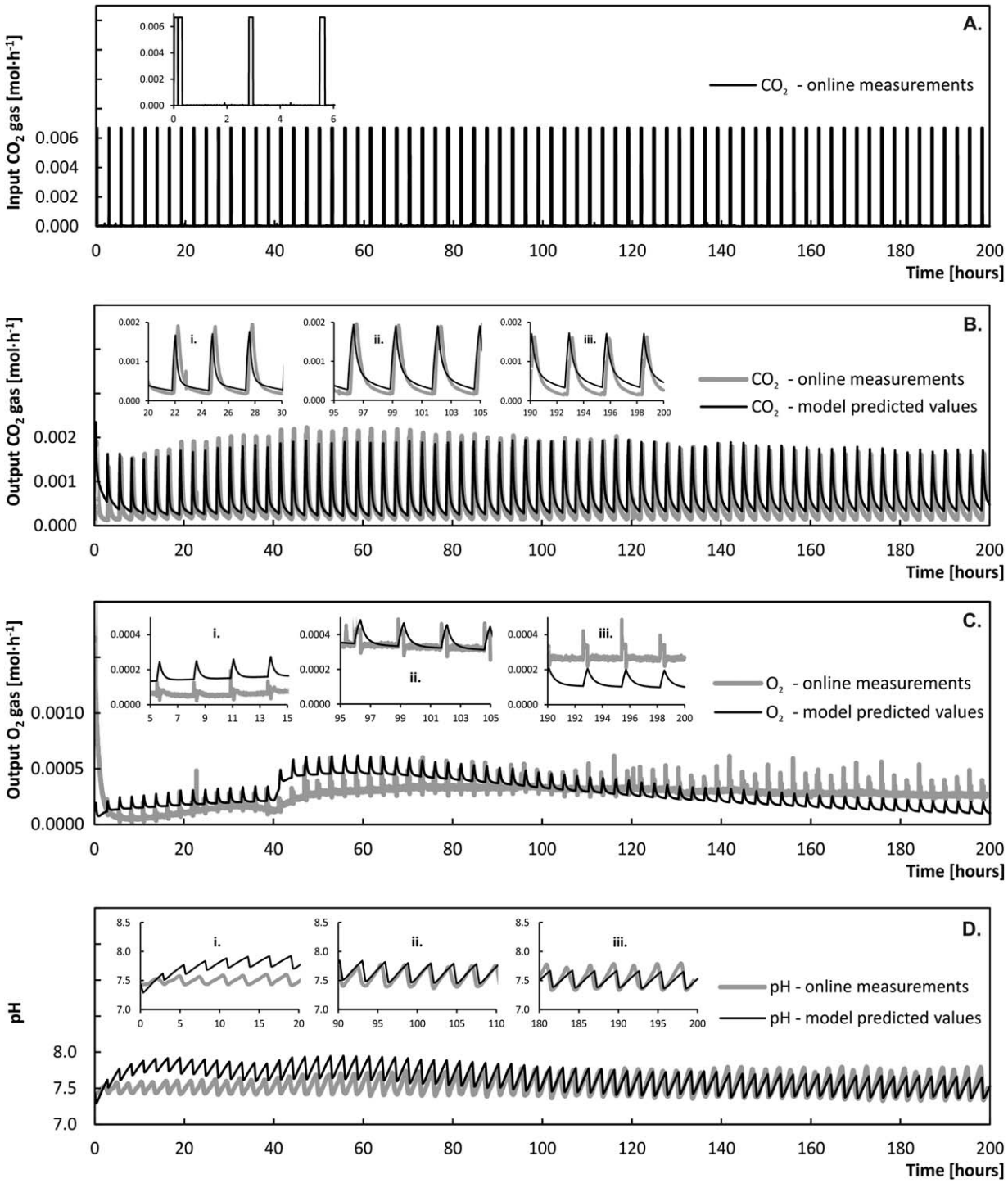

Figure 4. Dynamics of the variables measured online in a photoautotrophic batch culture operated at 110 μmol m^{-2} s^{-1} incident light intensity.

The input CO_2 gas was bubbled into the reactor to regulate the pH by means of a pulse width modulation controller, its flow rate (A) being measured by a dedicated flow meter. The output CO_2 gas flow rate (B—gray line) and the output O_2 gas flow rate (C—gray line) are the product of their output molar fraction, measured with a mass spectrometer, and the total output gas measured with a dedicated gas flow meter. The pH was measured online with a specific electrode (D—gray line). The pulsed signal of $G_{in}^{CO_2}$, together with its corresponding experimental time, was used as input in the global model whose response was overlapped on the experimental data (B, C, and D—black line). The model was initialized with the values presented in Table 2 and its parameters are rendered in Table 1.

respectively) when the biomass concentration is very low. The thermodynamic model which predicts the pH is very sensitive and needs to be properly initialized. A proper initialization of the thermodynamic model, along with an accurate photosynthetic growth model, will result in an excellent capacity of prediction.

One particular incident is noteworthy and took place during the third day of operation (approximately between the

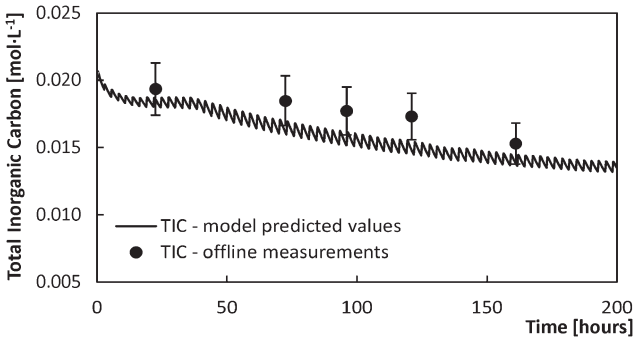

Figure 5. TIC consumption in a photoautotrophic batch culture operated at 110 μmol m^{-2} s^{-1} incident light intensity.

The concentration of TIC was measured offline by means of a specific analyzer (black dots). The response of the global photoautotrophic growth model (black line), integrated with the pulsed input CO_2 gas flow rate values and its corresponding experimental time, was compared with the offline measured values. The error bars were set to 10%. The model was initialized with the values presented in Table 2 and its parameters are rendered in Table 1.

50th and 70th h). As shown in the detail of Figure 6A, the input CO_2 gas lost its periodicity for a sufficient time to allow the prediction accuracy of the gas balance and pH models to be examined.

The output CO_2 gas (Detail 2, Figure 6B) and the output O_2 gas (Detail 2, Figure 6C) were very well predicted by the gas balance model, all the more so as the incident was projected on the exponential growth phase. The thermodynamic model was able to predict the pH (Figure 6D) over a wide range of operating points. From a biological point of view, the optimal pH for the growth of *Chlamydomonas reinhardtii* is 7.5,[37,38] and therefore, a pH controller needs to reject various disturbances rather than to work on other pH regimes; an important aspect to be considered for control purposes.

Model behavior

The pH is given by the quotas of the nine chemical species that form the $NH_3-CO_2-H_2O$ multisolute system, which, in their turn, are implicit functions of the state variables. The global photoautotrophic growth model is sensitive to a series of inputs, namely q_0, D, $G_{in}^{CO_2}$, $G_{in}^{O_2}$, $G_{in}^{N_2}$, and T, which affect the radiative, biological, and thermodynamic models, and consequently the pH. To investigate the response of the global photoautotrophic growth model to these input variables, a series of scenarios were considered for numerical simulation. The global photoautotrophic growth model was initialized with the values presented in Table 2.

The simulations were run for a period of 30 days, of which 10 days were assigned to batch regime ($D = 0$ h^{-1}) and the remaining 20 days to continuous regime ($D = 0.05$ h^{-1}). The value assigned to dilution in continuous mode corresponds to the maximal productivity of microalgal biomass that could be obtained in the photobioreactor under study, as shown in Ifrim et al.[39]

Various laboratory studies have been conducted on artificially lit photobioreactors, where the values assigned to the incident light intensities are constant. However, a sustained effort is now being made to operate the photobioreactors under solar light and, therefore, the mathematical models must give accurate predictions even when the incident light intensity, q_0, varies. Thus, q_0 varied between 0 and 1000 μmol m^{-2} s^{-1} throughout the entire simulation period, as illustrated in Figure 7. The light profile corresponded to the positive alternation of a sinusoidal signal with 700 μmol m^{-2} s^{-1} amplitude, 24-h period, −2.1 rad phase angle, and 300 μmol m^{-2} s^{-1} reference line. The signal is describing a summer day with approximately 15-h daylight at a latitude around 45 degrees north. The day/night cycle also causes temperature variations of up to 20°C as illustrated in Figure 7.[40] However, most of the simulations were run at a constant temperature of 25°C, unless explicitly stated otherwise.

Figure 8 displays the time evolution of biomass in both batch and continuous regimes under solar light conditions. From a mathematical point of view, the biomass concentration is altered only by two inputs, namely q_0 and D, as the specific growth rate (9) is expressed as a function of irradiance while other nutrients (e.g., TIC, TIN, etc.) are considered nonlimiting. To describe nutrient limiting phenomena or temperature effect on the growth kinetics, the model has to be enriched without needing to modify its structure. As it can be seen in Figure 8, under solar light conditions, the biomass concentration reaches approximately 2 g L^{-1} after 10 days of batch cultivation, and stabilizes at approximately 0.3 g L^{-1} in open loop, after a transitory phase of about 80 h. However, if closed loop control is aimed at, D can be upper bounded to shorten the transitory phase at positive steps and lower bounded to avoid the reactor's washout. A broader discussion on the response of the system to various dilution rates can be found in Ifrim et al.[39]

Even though the biomass growth is governed exclusively by irradiance, its dynamic expression is central to the global photoautotrophic growth model, whereas the consumption of TIC and TIN, and the production of O_2, are functions of the volumetric growth rate (7) and the rest of the variables are explicit functions of these states. The pH is thus sensitive to D and q_0, but is also strongly affected by the CO_2 feeding flow rate, $G_{in}^{CO_2}$, as described previously. Inorganic carbon is also provided through the culture media, representing a known disturbance. $G_{in}^{CO_2}$ was maintained at 0.0037 mol h^{-1} (50% aperture of the proportional valve) throughout the batch regime and half of the continuous regime, and reduced to 0 mol h^{-1} during the last 10 days of continuous cultivation, to examine the magnitude of the disturbance caused by the culture medium (Figure 9). In batch mode, the pH decreases because the biomass reaches a stationary phase and the amount of $CO_{2,aq}$ required for growth diminishes. In continuous mode, the system is maintained in a quasi-steady state at a pH of around 7. During the last 10 days, when no CO_2 was added to the culture broth, the pH increased, as expected, to around 9. The concentration of TIC in the culture medium was of 0.02 mol L^{-1}, but it can be enriched (to ~0.06 mol L^{-1}) so that the pH to be neutral in open loop without further CO_2 addition. The disadvantage of this type of auxostatic pH control is that the inorganic carbon from the culture medium is only partially consumed. On the other hand, the CO_2 is not completely dissolved in water and a significant amount is retrieved in the output gas. The pH variation over a day/night cycle is of approximately 0.5 units, but optimized protocols can be applied to reduce the CO_2 addition during the night.

TIC and TIN kinetics, which are inversely related to X, are displayed in Figures 10A and 11A. The addition of both

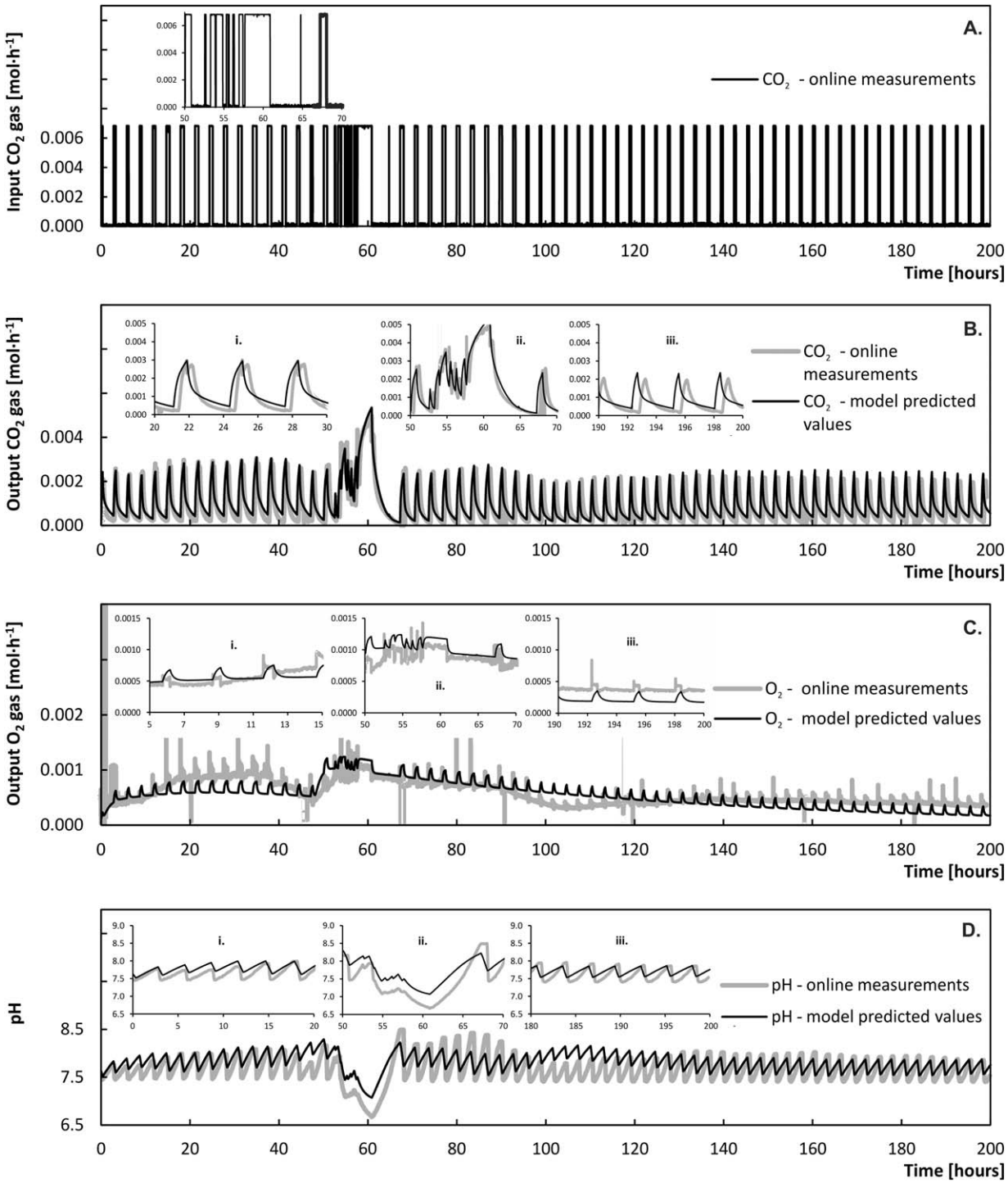

Figure 6. Dynamics of the variables measured online in a photoautotrophic batch culture operated at 300 μmol m^{-2} s^{-1} incident light intensity.

The input CO_2 gas was bubbled into the reactor to regulate the pH by means of a pulse width modulation controller, its flow rate (A) being measured by a dedicated flow meter. The output CO_2 gas flow rate (B—gray line) and the output O_2 gas flow rate (C—gray line) are the product of their output molar fraction, measured with a mass spectrometer, and the total output gas measured with a dedicated gas flow meter. The pH was measured online with a specific electrode (D—gray line). The pulsed signal of $G_{in}^{CO_2}$, together with its corresponding experimental time, was used as input in the global model whose response was overlapped on the experimental data (B, C, and D—black line). The model was initialized with the values presented in Table 2 and its parameters are rendered in Table 1.

HCO_3^- from fresh culture medium and gaseous CO_2 (Figure 10A) has the effect of maintaining the initial concentration of TIC unchanged. The TIC system depends on pH and below values of ~6.3 pH units the dominant species is $CO_{2,aq}$, between ~6.3 and ~10.3 HCO_3^- is the dominant species, whereas above ~10.3 CO_3^{2-} will become dominant. At a pH higher than ~8.2, no $CO_{2,aq}$ is present in the culture broth, but many species of microalgae are able to consume

Table 2. Initial Conditions Used for the Numerical Simulation of the Global Photoautotrophic Growth Model

Variable at t = 0[a]	Value	Unit
Biomass conc. – $X(0)$	0.200	$g \cdot L^{-1}$
TIN conc. – $c_{TIN}(0)$	0.027	$mol \cdot L^{-1}$
TIC conc. – $c_{TIC}(0)$	0.020	$mol \cdot L^{-1}$
Dissolved O_2 conc. – $c_{O_2}(0)$	0.000	$mol \cdot L^{-1}$
Output CO_2 molar fraction – $y_{out}^{CO_2}(0)$	0.005	–
Output O_2 molar fraction – $y_{out}^{O_2}(0)$	0.005	–
Output N_2 molar fraction – $y_{out}^{N_2}(0)$	0.990	–
Output gas – $G_{out}(0)$	0.2452	$mol \cdot h^{-1}$
Dissolved CO_2 conc. – $c_{CO_2}(0)$	1.32E-2	$mol \cdot L^{-1}$
Bicarbonate conc. – $c_{HCO_3^-}(0)$	1.11E-3	$mol \cdot L^{-1}$
Carbonate conc. – $c_{CO_3^{2-}}(0)$	5.69E-3	$mol \cdot L^{-1}$
Ammonia conc. – $c_{NH_3}(0)$	6.98E-3	$mol \cdot L^{-1}$
Ammonium conc. – $c_{NH_4^+}(0)$	2.00E-2	$mol \cdot L^{-1}$
Carbamate conc. – $c_{NH_2COO^-}(0)$	1.71E-5	$mol \cdot L^{-1}$
Hydroxyl conc. – $c_{OH^-}(0)$	8.24E-6	$mol \cdot L^{-1}$
Hydrogen conc. – $c_{H^+}(0)$	3.16E-8	$mol \cdot L^{-1}$
pH – pH(0)	7.500	-

[a]The initial values used for numerical simulations represent the real experimental concentrations used also for the above-described validation of the global photoautotrophic model with experimental data, thus $c_{TIN,i} \equiv c_{TIN}(0)$ and $c_{TIC,i} \equiv c_{TIC}(0)$.

HCO_3^- for growth. Figure 10B shows the proportion of each inorganic carbonaceous species of TIC in the culture conditions described above.

The TIN system also depends on pH, and above values of ~9.3, the dominant species is NH_3. Figure 11B illustrates the proportion of each inorganic nitrogenous species of TIN, in the culture conditions described above. NH_2COO^- is part of both TIC and TIN systems, but is present in the culture broth in extremely low concentration. Its concentration is ~0.01% of TIC at neutral pH and increases to ~0.3% of TIC at pH values higher than 8, as a result of NH_3 accumulation (5).

Temperature is another input that influences the global photoautotrophic growth model, the equilibrium constants,

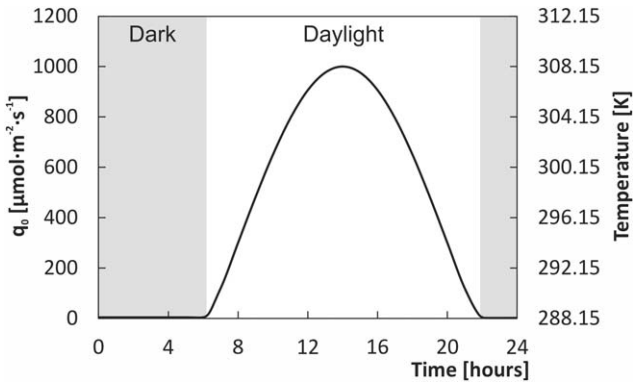

Figure 7. Day/night variation of incident light intensity and temperature.

To investigate the behavior of the global model under solar light, q_0 was varied between 0 and 1000 μmol m^{-2} s^{-1} throughout the entire simulation period. The incident light profile corresponds to the positive alternation of a sinusoidal signal with 700 μmol m^{-2} s^{-1} amplitude, 24-h period, −2.1 rad phase angle, and 300 μmol m^{-2} s^{-1} reference line. The signal describes a summer day with approximately 15-h daylight at a latitude around 45 degrees north. The day/night cycle also causes temperature variations of up to 20°C. The sinusoidal signals of q_0 and T (only for the cases explicitly mentioned) are inputs for the global model.

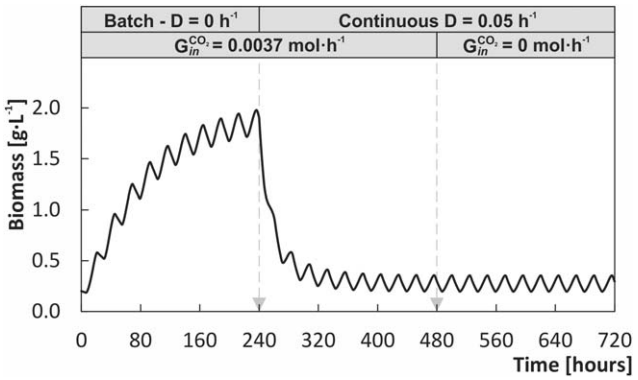

Figure 8. Numerical simulation of biomass dynamics in solar photobioreactors.

Numerical simulations were run for a period of 30 days, of which 10 days were assigned to batch regime ($D = 0$ h^{-1}) and the remaining 20 days to continuous regime ($D = 0.05$ h^{-1}). The model that uses as inputs sinusoidal signals for q_0 and T (Figure 7) and step signals for D was initialized with the values presented in Table 2. The parameters of the model are listed in Table 1.

the activity coefficients and the gas balance model being functions of temperature. Nevertheless, a 20°C temperature variation (Figure 7) leads to negligible changes in the chemical species of the $NH_3-CO_2-H_2O$ multisolute system, which, expressed in terms of pH, give mismatches of up to 0.3 units, especially at high pH (Figure 9—gray line).

Activity coefficients and water activity account the deviation from the ideal behavior of the chemical species concentration in the mixture, being complex functions of ionic strength and temperature, and therefore, not constant in time. However, their variation is extremely low and can be

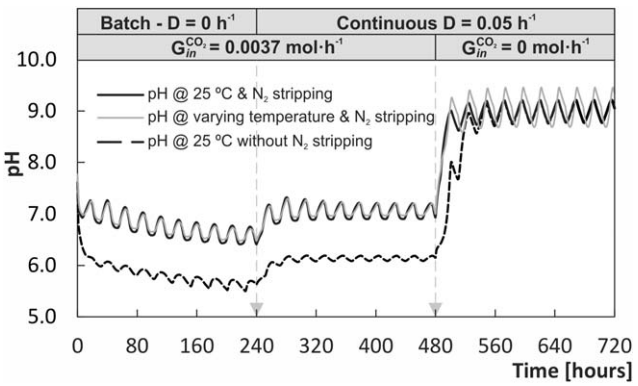

Figure 9. Numerical simulation of pH dynamics in solar photobioreactors.

Numerical simulations were run for a 30 days period under various operating conditions to analyze the dynamics of the pH. In addition to q_0 and D, a step signal was associated to $G_{in}^{CO_2}$, thus $G_{in}^{CO_2}$ was maintained at 0.0037 mol h^{-1} (50% aperture of the proportional valve) throughout the batch regime and half of the continuous regime, and reduced to 0 mol h^{-1} during the last 10 days of continuous cultivation, to examine the magnitude of the disturbance caused by the culture medium containing $NaHCO_3$ (black continuous line). The latter, run at constant temperature, was compared with a simulation with varying day/night temperature (gray continuous line). As $G_{in}^{N_2}$ has a stripping effect over the CO_2, a third simulation was run at $G_{in}^{N_2} = 0$ mol h^{-1} (black dash line). The parameters of the model and the initial values of its variables are listed in Tables 1 and 2.

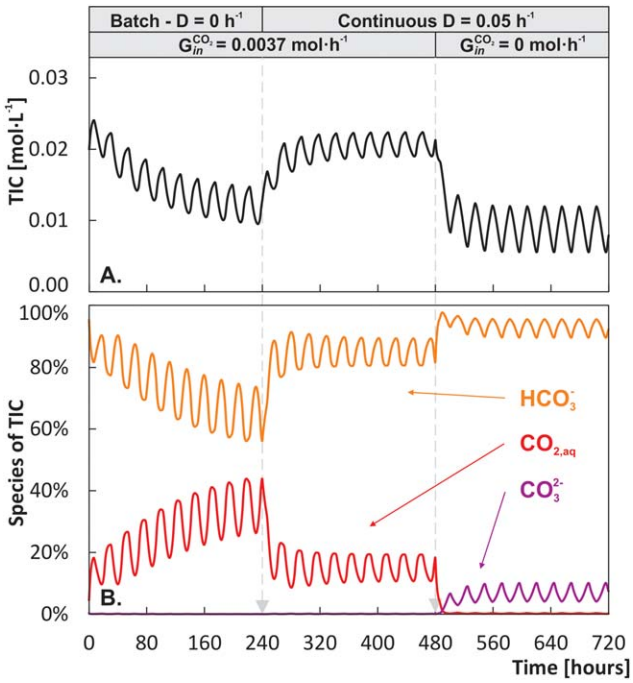

Figure 10. Numerical simulation of TIC dynamics in solar photobioreactors.

Numerical simulations were run for a 30 days period under various operating conditions to investigate the dynamics of (A) the TIC, which represents the sum of (B—red line) $CO_{2,aq}$, (B—orange line) HCO_3^-, (B—purple line) CO_3^{2-}, and NH_2COO^- (not displayed because it is present in extremely low concentrations). The contribution of each inorganic carbonaceous species to TIC is expressed in percents to relate them with the dynamics of the pH. The parameters of the model and the initial values of its variables are listed in Tables 1 and 2. [Color figure can be viewed in the online issue, which is available at wileyonlinelibrary.com.]

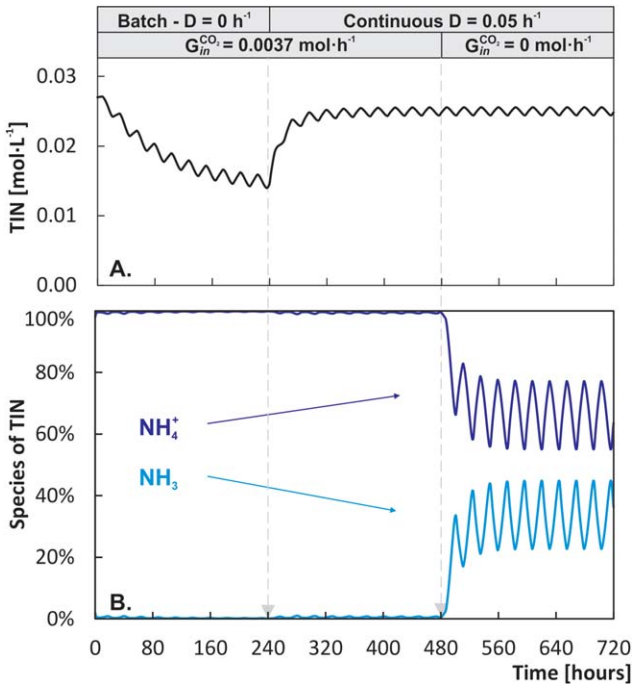

Figure 11. Numerical simulation of TIN dynamics in solar photobioreactors.

Numerical simulations were run for a 30 days period under various operating conditions to examine the dynamics of (A) the TIN, which represents the sum of (B—cyan line) NH_3, (B—dark blue line) NH_4 and NH_2COO^- (not displayed because it is present in extremely low concentrations). The contribution of each inorganic nitrogenous species to TIN is expressed in percents to relate them with the dynamics of the pH. The parameters of the model and the initial values of its variables are listed in Tables 1 and 2. [Color figure can be viewed in the online issue, which is available at wileyonlinelibrary.com.]

expressed as average values (Table 3). Whether they are recalculated for each integration step or used as average values, the pH profiles have very low mismatches of at most 0.02 pH units—@ pH = 6 ÷ 10 and $T = 15 \div 35$°C.

If the thermodynamic model is to be reduced, the activity coefficients can be neglected (i.e., $\gamma_i = 1$), working directly with concentrations, case in which the mismatch is of at most 0.1 pH units—@ pH = 6 ÷ 10 and $T = 15 \div 35$°C.

When the temperature is an unknown disturbance and the activity coefficients are ignored, the mismatch could be higher than 0.5 pH units, and therefore, besides a good growth model, it is necessary to have a good thermodynamic model to precisely predict the pH.

The output molar fractions $y_{\text{out}}^{CO_2}$, $y_{\text{out}}^{O_2}$, and $y_{\text{out}}^{N_2}$ are displayed in Figure 12. CO_2 is partially dissolved in water and, although it is consumed by microalgae during the day, more than 50% is found in the output gas. On the other hand, during the night, the CO_2 is found entirely in the output gas. O_2 is produced during water photolysis and, whether it is dissolved or in gaseous form, it is an excellent indicator of the photosynthetic growth. Thus, $y_{\text{out}}^{O_2}$ is null during the night, when r_x is negative because the microalgae consume energy for respiration, the peak being at midday. N_2 has a lower solubility in water, its flow remaining unchanged throughout the entire simulation period.

The dynamics of the gases also influence the pH in the sense that N_2 and O_2 are less dissolved in water, and have a stripping effect on CO_2. Stripping CO_2 from the culture causes the pH to increase. In the experimental installation presented here, the N_2 is used as vector gas, the mass spectrometer requiring a specific gas flow to measure its composition. When the reactor is mechanically stirred and measurement of the gas composition is not required, pure CO_2 can be bubbled into the culture. To investigate the magnitude of the stripping effect on the pH, the simulations ran at a constant temperature of 25°C and $G_{\text{in}}^{N_2} = 0.0245$ mol h^{-1} were iterated for the same temperature and $G_{\text{in}}^{N_2} = 0$ mol h^{-1}

Table 3. Activity Coefficients

Activity coefficient	Recommended average values for pH < 6	Recommended average values for pH 6 ÷ 10
$\overline{\gamma}_{NH_3}$	1.00	1.00
$\overline{\gamma}_{NH_4^+}$	0.94	0.88
$\overline{\gamma}_{NH_2COO^-}$	0.94	0.88
$\overline{\gamma}_{CO_2}$	1.00	1.00
$\overline{\gamma}_{HCO_3^-}$	0.93	0.86
$\overline{\gamma}_{CO_3^{2-}}$	0.76	0.57
$\overline{a}_w$	1.00	1.00
$\overline{\gamma}_{OH^-}$	0.94	0.88
$\overline{\gamma}_{H^+}$	0.93	0.87

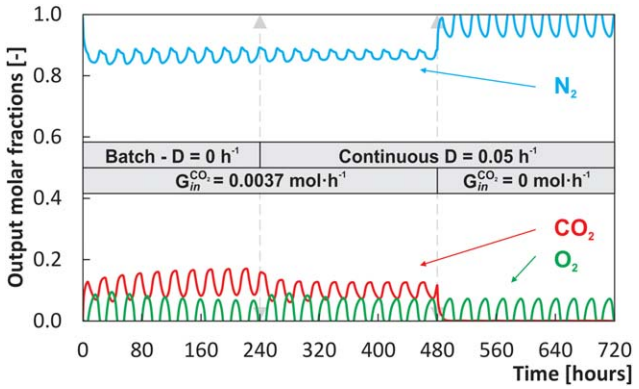

Figure 12. Numerical simulation of output CO_2, O_2, and N_2 molar fractions in solar photobioreactors.

Numerical simulations were run for a 30 days period under various operating conditions to study the dynamics of the output CO_2 (red line), O_2 (green line), and N_2 (cyan line) molar fractions. The global model was integrated with sinusoidal input signal for q_0 and step signals for D, T, $y_{out}^{CO_2}$, and $y_{out}^{N_2}$, the scenario with $G_{in}^{N_2} = 0$ mol h^{-1} (Figure 12—black dash line) being not displayed. The parameters of the model and the initial values of its variables are listed in Tables 1 and 2. [Color figure can be viewed in the online issue, which is available at wileyonlinelibrary.com.]

(Figure 9—black dashed line), the result showing that the pH decreases with almost 2 units.

Other operating protocols require CO_2 enriched air, which plays an additional role in the homogenization of the culture. In this case, the pH is expected to be higher because the CO_2 stripping effect is even more intense. $G_{in}^{O_2}$ and $G_{in}^{N_2}$ are thus inputs with increased influence over the entire system and hence over the pH.

It can be concluded that all identified inputs (i.e., q_0, D, $G_{in}^{CO_2}$, $G_{in}^{O_2}$, $G_{in}^{N_2}$, and T) have a strong influence over the system and ultimately on the pH. Some of them can be designated as control variables (i.e., q_0—only for artificially lit photobioreactors, D and $G_{in}^{CO_2}$), whereas others can be treated as known disturbances (i.e., $G_{in}^{O_2}$, $G_{in}^{N_2}$, and T).

Conclusions

A global photoautotrophic growth model was developed and experimentally validated on a laboratory pilot plant, together with an analysis in simulation to demonstrate its applicability for monitoring and control purposes. In addition, the coupling between a radiative model, a biological model, and a thermodynamic model led to an accurate prediction of the dynamic evolution of the pH which is a key feature in microalgae culture. This allows its use for designing valuable model-based control strategies.[39]

The model was validated on a torus reactor inoculated with *Chlamydomonas reinhardtii* cells, but it can be used for other devices or organisms on condition that the optical and kinetic parameters are reidentified, together with some transfer parameters that depend strictly on the shape of the reactor ($(K_La)_{O_2}$ and $H_{O_2|CO_2}$).

The model presented here accurately describes the dynamic evolution of the pH in nonlimiting conditions with respect to nutrients (TIN, TIC), being validated at constant temperature and incident light flux. Yet, it returned good results in simulation even when the temperature and the incident light flux varied. The studies carried out in practice and in simulation emphasized that the pH is equally governed by the biological activity of microalgae, the dynamics of the gases and also the chemical properties of the culture broth. The influences of nutrient concentration as well as the temperature effect on the microorganism growth are crucial for extending the model to solar photobioreactors and these are topics of ongoing research.

Acknowledgments

The authors acknowledge the financial support of POSDRU 6/1.5/S/15–6583, acronym SIMBAD and of SOLAR-H_2 EU–212508, the experimental work provided by Benoit Degrenne and the language help provided by Mihaela-Alina Ifrim.

Literature Cited

1. Becker W. Microalgae in human and animal nutrition. In: Richmond A, editor. *Handbook of Microalgal Culture*. Oxford: Blackwell, 2004:312–351.
2. Grossman AR, Lohr M, Im CS. *Chlamydomonas reinhardtii* in the landscape of pigments. *Annu Rev Genet*. 2004;38:19–73.
3. Spolaore P, Joannis-Cassan C, Duran E, Isambert A. Commercial applications of microalgae. *J Biosci Bioeng*. 2006;101:87–96.
4. Doshi H, Seth C, Ray A, Kothari IL. Bioaccumulation of heavy metals by green algae. *Curr Microbiol*. 2008;56:246–255.
5. Kong QX, Li L, Martinez B, Chen P, Ruan R. Culture of microalgae *Chlamydomonas reinhardtii* in wastewater for biomass feedstock production. *Appl Biochem Biotechnol*. 2010;160:9–18.
6. Chisti Y. Biodiesel from microalgae. *Biotechnol Adv*. 2007;25:294–306.
7. Brennan L, Owende P. Biofuels from microalgae—a review of technologies for production, processing, and extractions of biofuels and co-products. *Renew Sust Energy Rev*. 2010;14:557–577.
8. Fouchard S, Pruvost J, Degrenne B, Legrand J. Investigation of H2 production using the green microalga *Chlamydomonas reinhardtii* in a fully controlled photobioreactor fitted with on-line gas analysis. *Int J Hydrogen Energy*. 2008;33:3302–3310.
9. Degrenne B, Pruvost J, Legrand J. Effect of prolonged hypoxia in autotrophic conditions in the hydrogen production by the green microalga *Chlamydomonas reinhardtii* in photobioreactor. *Bioresour Technol*. 2010;102:1035–1043.
10. Cornet JF, Dussap CG, Gros JB. Conversion of radiant light energy in photobioreactors. *AIChE J*. 1994;40:1055–1066.
11. Cornet JF, Dussap CG, Gros JB. Kinetics and energetics of photosynthetic micro-organisms in photobioreactors. Application to Spirulina growth. In: Scheper T, editor. *Bioprocess and Algae Reactor Technology, Apoptosis*. Berlin/Heidelberg: Springer, 1998:153–224.
12. Molina Grima E, Acién Fernández FG, García Camacho F, Chisti Y. Photobioreactors: light regime, mass transfer, and scaleup. *J Biotechnol*. 1999;70:231–247.
13. Rubio FC, Fernandez FG, Perez JA, Camacho FG, Grima EM. Prediction of dissolved oxygen and carbon dioxide concentration profiles in tubular photobioreactors for microalgal culture. *Biotechnol Bioeng*. 1999;62:71–96.
14. Pruvost J, Legrand J, Legentilhomme P, Muller-Feuga A. Simulation of microalgae growth in limiting light conditions: flow effect. *AIChE J*. 2002;48:1109–1120.
15. Pottier L, Pruvost J, Deremetz J, Cornet JF, Legrand J, Dussap CG. A fully predictive model for one-dimensional light attenuation by *Chlamydomonas reinhardtii* in a torus photobioreactor. *Biotechnol Bioeng*. 2005;91:569–582.
16. Cornet JF, Dussap CG. A simple and reliable formula for assessment of maximum volumetric productivities in photobioreactors. *Biotechnol Prog*. 2009;25:424–435.
17. Fouchard S, Pruvost J, Degrenne B, Titica M, Legrand J. Kinetic modeling of light limitation and sulfur deprivation effects in the induction of hydrogen production with *Chlamydomonas reinhardtii*: part I. Model development and parameter identification. *Biotechnol Bioeng*. 2009;102:232–245.
18. Takache H, Christophe G, Cornet JF, Pruvost J. Experimental and theoretical assessment of maximum productivities for the micro-

algae *Chlamydomonas reinhardtii* in two different geometries of photobioreactors. *Biotechnol Prog*. 2010;26:431–440.
19. Pruvost J, Cornet JF, Goetz V, Legrand J. Modeling dynamic functioning of rectangular photobioreactors in solar conditions. *AIChE J*. 2011;57:1947–1960.
20. Derks PWJ, Versteeg GF. Kinetics of absorption of carbon dioxide in aqueous ammonia solutions. *Energy Procedia*. 2009;1:1139–1146.
21. Jilvero H, Normann F, Andersson K, Johnsson F. Thermal integration and modelling of the chilled ammonia process. *Energy Procedia*. 2011;4:1713–1720.
22. Colt J, Watten B, Rust M. Modeling carbon dioxide, pH, and unionized ammonia relationships in serial reuse systems. *Aquacult Eng*. 2009;40:28–44.
23. Pruvost J, Pottier L, Legrand J. Numerical investigation of hydrodynamic and mixing conditions in a torus photobioreactor. *Chem Eng Sci*. 2006;61:4476–4489.
24. Edwards TJ, Maurer G, Newman J, Prausnitz JM. Vapour-liquid equilibria in multicomponent aqueous solutions of volatile weak electrolytes. *AIChE J*. 1978;24:966–975.
25. Harris EH. *The Chlamydomonas Sourcebook. Vol. 1. Introduction to Chlamydomonas and Its Laboratory Use*, 2nd ed. San Diego, CA: Academic Press, 2009.
26. Jaworski Z, Czernuszewicz M, Gralla L. A comparative study of thermodynamic electrolyte models applied to the Solvay soda system. *Chem Process Eng*. 2011;32:135–154.
27. Pitzer KS. Thermodynamics of electrolytes. *I. Theoretical basis and general equations. J Phys Chem*. 1973;77:268–277.
28. Pruvost J, Van Vooren G, Le Gouic B, Couzinet-Mossion A, Legrand J. Systematic investigation of biomass and lipid productivity by microalgae in photobioreactors for biodiesel application. *Bioresour Technol*. 2011;102:150–158.
29. Loubière P, Cocaign-Bousquet M, Matos J, Goma G, Lindley ND. Influence of end-products inhibition and nutrients limitations on the growth of *Lactococcus lactis subsp. lactis. J Appl Microbiol*. 1997; 82:95–100.
30. Roels JA. *Energetics and Kinetics in Biotechnology*. Amsterdam: Elsevier Biomedical Press, 1983.
31. Schumpe A. Gas solubilities in biomedia. In: Rehm HJ, Reed G, editors. *Biotechnology*. Vol. 2. Weinheim: VCH Publishers, 1985: 160–170.
32. Zemaitis JF, Clark DM, Rafal M, Scrivner NC. *Handbook of Aqueous Electrolyte Thermodynamics*. New York: DIPPD, AIChe, 1986.
33. Dochain D. *Automatic Control of Bioprocesses*. Great Britain: Wiley, 2008.
34. Denny MW. *Air and Water. The Biology and Physics of Life's Media*. Princeton, NJ: Princeton University Press, 1993.
35. Shah YT, Kelkar BG, Godbole SP, Deckwer WD. Design parameters estimations for bubble column reactors. *AIChE J*. 1982;28:353–379.
36. Mirón AS, Camacho FG, Gómez AC, Grima EM, Chisti Y. Bubble--column and airlift photobioreactors for algal culture. *AIChE J*. 2000; 46:1872–1887.
37. Kong QX, Li L, Martinez B, Chen P, Ruan R. Culture of microalgae *Chlamydomonas reinhardtii* in wastewater for biomass feedstock production. *Appl Biochem Biotechnol*. 2010;160:9–18.
38. Kosourov S, Seibert M, Ghirardi ML. Effects of extracellular pH on the metabolic pathways in sulfur-deprived, H2-Producing *Chlamydomonas reinhardtii* Cultures. *Plant Cell Physiol*. 2003;44:146–155.
39. Ifrim GA, Titica M, Barbu M, Boillereaux L, Cogne G, Caraman S, Legrand J. Multivariable feedback linearizing control of *Chlamydomonas reinhardtii* photoautotrophic growth process in a torus photobioreactor. *Chem Eng J*. 2013;218:191–203.
40. Goetz V, Le Borgne F, Pruvost J, Plantard G, Legrand J. A generic temperature model for solar photobioreactors. *Chem Eng J*. 2011; 175:443–449.

Manuscript received Jan. 22, 2013, and revision received Sept. 30, 2013.